

High-power MEMS switch enabled by carbon-nanotube contact and shape-memory-alloy actuator

Masoud Dahmardeh¹, Mohamed Sultan Mohamed Ali^{1,2}, Tanveer Saleh^{1,3}, Tee Min Hian⁴, Mehran Vahdani Moghaddam¹, Alireza Nojeh^{**1}, and Kenichi Takahata^{*1}

¹Department of Electrical and Computer Engineering, University of British Columbia, Vancouver, British Columbia V6T 1Z4, Canada

²Faculty of Electrical Engineering, Universiti Teknologi Malaysia, Skudai 81310, Johor, Malaysia

³Department of Mechatronics Engineering, International Islamic University Malaysia, Kuala Lumpur 50728, Malaysia

⁴Department of Mechanical Engineering, University of British Columbia, Vancouver, British Columbia V6T 1Z4, Canada

Received 4 October 2012, revised 27 January 2013, accepted 30 January 2013

Published online 25 February 2013

Keywords actuators, carbon nanotubes, microelectromechanical systems, shape-memory alloys, switches

* Corresponding author: e-mail takahata@ece.ubc.ca, Phone: +1 604 827 4241, Fax: +1 604 822 5949

** e-mail anojeh@ece.ubc.ca, Phone: +1 604 827 4346, Fax: +1 604 822 5949

A forest of vertically aligned carbon nanotubes (CNTs) is integrated as an electrical contact material with a high-power, normally-open switch based on micro-electro-mechanical systems (MEMS) technology. A shape-memory-alloy (SMA) cantilever is thermally actuated to enable switching between the movable CNT forest and the copper electrode formed on the SMA. The out-of-plane SMA actuator provides high forces to enable distributed contacts with the CNT forest, achieving low

contact resistances and high ON/OFF resistance ratios. The ON state of the switch shows contact resistances as low as 35 Ω with a dependence on the operating current. The device operation is performed with over 5-W input powers. Long-term operation with more than 1×10^6 switching cycles is demonstrated. The results indicate that a combination of the CNT-based contact and the SMA actuator may be a promising path to realizing reliable MEMS contact switches for high-power applications.

© 2013 WILEY-VCH Verlag GmbH & Co. KGaA, Weinheim

1 Introduction Micro-electro-mechanical switches have benefits over solid-state switches such as low OFF-state leakage current, high ON/OFF resistance ratio, high breakdown voltage, and low distortion [1–3]. Due to the physical limitations of power transistors, high-power switches based on micro-electro-mechanical-systems (MEMS) technology have been attracting more attention [4, 5]; however, there are still essential issues in this application area [5]. Reliability and lifetime of the contact are among the challenges of MEMS contact switches, especially for the above area. The contact resistance depends on a variety of factors, including the contact force, contact roughness, and the material properties [6]. Typical contact materials used for MEMS contact switches are pure metals such as gold [2, 7], nickel [8], and aluminum [9]. The actual contact area of these metallic contacts tends to be limited by the presence of discrete contact points and thus much smaller than the designed area [10, 11]. Furthermore, these point contacts cause welding, shorting, and stiction failures [12].

For instance, metallic MEMS switches were reported to fail after cycles in the orders of 10^3 [7] and 10^4 [8] due to damages at localized point contacts. A variety of contact designs have been reported to improve device performance toward high power applications, including a ball-grid-array contact [13], a liquid-metal wetted contact [14], a gold contact with a meshed drain electrode [15], and a ruthenium contact switch with a corrugated diaphragm [6]. The use of an arc-suppression circuit was also reported to enable arcless operation of microrelays for high power applications [16]. Actuation-assisted release mechanisms [5, 17, 18] have also been actively studied to address stiction related failures in MEMS contact switches.

The carbon-nanotube (CNT) forest is a vertically aligned, densely packed array of CNTs with heights ranging from a few micrometers to several millimeters [19]. Because of its large surface area [10] and promising electrical, mechanical, and thermal properties [20], this is a good candidate for a more reliable contact material for MEMS

switches. For example, CNTs have been reported to have a high current capacity of more than 10^9 A cm^{-2} [21, 22]. Multi-walled CNTs exhibit a resistivity as low as $10^{-4} \Omega \text{ cm}^2$ [23]. They also exhibit very high thermal conductivity ($1400 \text{ W m}^{-1} \text{ K}^{-1}$) and operational temperatures (up to 2000 K) [24]. The junctions of CNTs and metallic electrodes have been reported to show resistance levels of $10^4\text{--}10^9 \Omega$ [25]. High-density CNT forests for interconnect applications [26] as well as a wafer-scale growth of patterned forests [27] were reported. There have been efforts to integrate CNTs with MEMS [28–36]. A normally closed MEMS switch that uses a contact of two CNT forests has been reported [37]. The design of this switch is based on electrostatic actuation and requires high voltages to detach the two forests off and achieve the OFF state. The condition in the ON state that no force is actively applied to the contact may limit the ability to minimize the contact resistance. In addition, the device layout based on in-plane actuation can occupy more chip space.

MEMS switches have also been reported with other actuation methods, including electrothermal [38, 39], magnetic [40], and piezoelectric principles [41]. Electrothermal actuation generally offers large forces, large displacements, and ease of on-chip integration. The former two features are advantageous in making stable, low-resistance contacts in the ON state and high isolation in the OFF state, respectively [38]. Shape-memory-alloy (SMA) actuators have been widely investigated in MEMS [42–44]. As one type of thermal (often electrothermal) actuators, they offer similar characteristics together with high fatigue resistance to cyclic operations, which is also advantageous for switching applications [45, 46]. Out-of-plane actuation can be easily achieved with simple SMA structures as opposed to typical electrothermal actuators that have in-plane actuation schemes, potentially enabling a small device footprint. In general, SMA actuation is slow compared to other principles; however, this may not be a major issue for high-power switching applications [4, 47]. Moreover, given the attractive features outlined above, SMA actuators may be a suitable choice for DC/low-frequency contact switches in the above application field.

In this paper, we report a normally open, SMA-based MEMS switch that is integrated with a CNT forest used as contact material. The characteristics of the electrical contact between the CNT forest and a metallic electrode are investigated along with their dependences on control parameters for the device operation. Results from high-current operation and long-term switching tests are reported as well. The outcome of these experiments suggests that the integration of SMAs and CNT forests is a promising path toward realizing a reliable MEMS contact switch for high-power applications.

2 Experimental Figure 1 shows the layout of the developed switch device and the SMA actuator component used in the device. The SMA has a cantilever structure as shown, being fabricated to bend upward in its martensitic

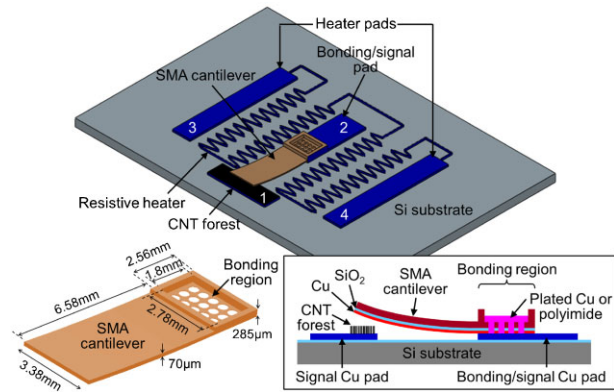


Figure 1 (online color at: www.pss-a.com) Schematic illustration of the top view of the contact switch device (top), along with the details of the SMA cantilever component with dimensions (bottom left) and a cross-sectional view of the device in the OFF state (bottom right).

(cold) state at room temperature and vertically actuated downward when it is heated and enters its austenite (hot) state [44]. Thus, the signal terminal 1 (CNT forest) and terminal 2 (bonding pad for SMA) indicated in Fig. 1 are disconnected in the cold state. As also shown in the figure, the cantilever is designed to have the bonding region with a cavity and perforations used for the bonding process. When the temperature of the SMA is elevated to exceed its threshold (austenite-phase) temperature, the cantilever is actuated and returns to its memorized flat shape. This thermal actuation is performed using resistive heaters integrated on the substrate (Si with a 2-µm-thick SiO₂ insulation layer) by passing a driving current between terminals 3 and 4. As the cantilever is actuated, it makes contact with the top surface of the CNT forest arranged underneath the cantilever, at which point the switch is closed (*i.e.*, terminals 1 and 2 are shorted). SMAs generally have relatively high resistivity levels. To minimize resistance at the contact and through the switch circuit, the bottom side of the SMA cantilever is coated with copper (with 200-nm thickness). The cantilever structure is bulk-micromachined in 300-µm-thick nickel-titanium SMA (so called Nitinol) sheets with a threshold temperature of 65 °C (Alloy M, Memory Metalle GmbH, Germany). Prior to copper coating, the bottom side of the structure is deposited with 4-µm-thick SiO₂ that works as a compressive reset layer for the SMA actuator, so that the cantilever bends toward the uncoated (top) side at room temperature due to the stress applied by the layer. When the SMA is heated beyond the threshold temperature, its phase-transition force overcomes the bending moment caused by the SiO₂ layer and makes the cantilever flat to push the CNTs downward, achieving good electrical contacts with the individual nanotubes. As heat is removed, the cantilever restores its cold-state shape by bending up, making the switch open.

A forest of multi-walled CNTs with a thickness range of 100–200 µm is directly grown on the heater substrate. To mechanically and thermally couple the SMA component

with the substrate on which a CNT forest is present, we have investigated two integration approaches, wet and dry methods. In the wet method, the bonding region of the SMA is coupled with the bonding pad on the substrate using photolithography-assisted copper electroplating [43]. This process requires the CNTs to become wet and then dried. In the other approach, the dry method, the SMA is directly fixed onto the bonding pad of the substrate using liquid polyimide (PI) by filling it in the cavity of the region and curing it to fix the cantilever. In this case, the CNT forest remains dry throughout the fabrication of the device. Images of the devices developed through the above dry and wet processes are shown in Fig. 2a and b, respectively. As can be seen in Fig. 2b, the forest that went through the wet process was densified, due to capillary effects [48, 49], forming random structures of bundled nanotubes. In contrast, as shown in Fig. 2a, the device fabricated through the dry process maintains the original forest structures and surfaces. As in typical CNT forests, the forests grown in this study had some level of thickness variation within each forest.

For the fabrication of the heater circuit and signal/bonding pads on the substrate, Cr (15 nm) and Cu (200 nm) layers were first e-beam evaporated on a lightly doped Si wafer with a 2- μm -thick SiO_2 layer. Photoresist (SPR 220-7, Rohm and Hass Co., PA, USA) was spin coated and patterned to define the layout of the heater and pads. Cu electroplating was performed for 50 μm of thickness over the exposed Cu layer within the photo-defined region, followed by striping the photoresist and etching away the Cr–Cu layers underneath. Al_2O_3 (10 nm) and Fe (1.5 nm) were then e-beam evaporated on the corresponding Cu pad through a shadow mask as the catalyst layer for the CNT growth. A

multi-walled CNT forest was synthesized for a height of up to 200 μm through ethylene-based atmospheric chemical vapor deposition (CVD) [50]. The SMA cantilever (Fig. 1) was shaped with chemical etching of the Nitinol sheet for thinning and then shaped with micro-electro-discharge machining (μEDM) using a commercial μEDM system (EM203, SmalTec International Inc., IL, USA) [44]. (This μEDM technique may also be used to planarize the top surface of the CNT forest and adjust its height [49, 50] to address the thickness variation of the forest discussed earlier.) The SiO_2 reset layer was deposited on the bottom side of the SMA cantilever with plasma-enhanced CVD at 350 $^\circ\text{C}$ while keeping it flat as the memorized state, followed by e-beam evaporation of the Cu layer on top of the reset layer. For bonding the SMA to the substrate, in the wet method, the component was fixed onto the substrate using an electroplating bonding technique [43]. After fixing the bonding region of the SMA using the SPR photoresist spin-coated on the substrate as a temporary adhesive (covering the CNT forest as well) followed by soft baking at 45 $^\circ\text{C}$ for 1 h, the photoresist on the region was exposed to ultraviolet light (the other regions were masked) and developed so that the SPR on top and in the perforations of the region was removed. This region was then electroplated with Cu for 120- μm thickness to bond the SMA to the substrate. The device was completed by dissolving the SPR in acetone, rinsing the device with isopropyl alcohol and deionized water, and drying it in air. In the dry method, the bonding region of the SMA was aligned to the bonding pad, and then liquid PI (HD-4010, HD Microsystems, DE, USA) was directly applied to the cavity and perforations and cured to complete the bonding.

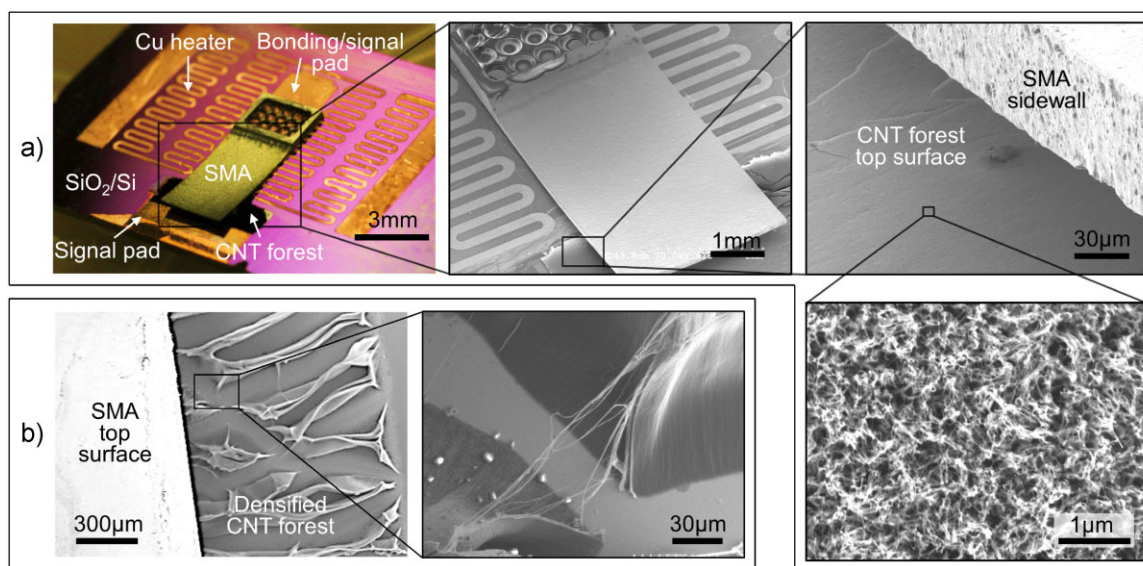


Figure 2 (online color at: www.pss-a.com) (a) Overall optical image of the dry-processed switch device and close-up scanning-electron-microscope (SEM) images showing the SMA structure and top surfaces of the CNT forest integrated into the device. (b) SEM images of the CNT forest in the device fabricated through the wet process, showing the densified structures of the CNTs that have lost their vertical alignment.

The experiments performed for the temporal control and long-term operations of the SMA actuator as well as the electrical measurements in these tests (to be discussed in the subsequent section) used a set-up centered on an electronic workstation board (NI ELVIS, National Instrument Co., TX, USA) coupled with LabVIEW programs. An amplifier was used to drive the heater of the devices using the signals generated by the board. The feedback loop used for the temporal control of the switch was established as follows: the heater driving current was increased while monitoring the contact resistance. As soon as the contact resistance dropped below a threshold level (set to be $10\text{ k}\Omega$ in the experiments), the heater current was terminated to cool the device and open the contact, after which the current was applied again to repeat the ON-OFF cycle. The displacement measurement of the SMA cantilever was performed using a laser displacement sensor (LK-G32, Keyence, ON, Canada) with a resolution of 10 nm and a spot size of $30\text{ }\mu\text{m}$.

3 Results and discussion We first evaluated the performance of the two types of devices with the densified and original CNT forests. Heating the device substrates to a temperature of $\sim 100\text{ }^\circ\text{C}$ or greater with a driving current of $0.5\text{--}0.9\text{ A}$ was observed to enable full deflections of the cantilevers. Figure 3a and b show the dependence of the contact resistance (probed between terminals 1 and 2) on the driving current for the wet- and dry-processed devices (both operated in air), respectively. The open resistances of these two devices were $20\text{ M}\Omega$ or more (not shown in the figures). The wet-processed device exhibited significantly higher contact resistance than the dry-processed one; the dry

one showed a resistance of $\sim 500\text{ }\Omega$ in repeated switching consistently, while the wet-bonded device showed a resistance of a few $\text{k}\Omega$ at the first contact and then even higher resistances (in the order of $10\text{ k}\Omega$) after that as depicted in Fig. 3a. The more resistive contact with the wet-processed device may be associated with the nonuniform (and probably more rigid) structures of the densified forest, potentially leading to a smaller actual contact area. The mismatch between the OFF-to-ON and ON-to-OFF paths in each result is presumably due to a hysteresis in thermomechanical response of SMA under a heating-cooling cycle [43]. Another possible cause of the mismatch could be related to the geometry of the individual CNTs that have somewhat wavy shapes; their tips can adhere to the cantilever surface due to the van der Waals force [51], potentially elongating the nanotube structures and maintaining the contacts during an early stage of the upward displacement of the cantilever, and then eventually detached from the surface. This type of the SMA cantilever used can exert very high actuation forces ($\sim 840\text{ mN}$ [44]) that are larger than those available with typical MEMS switches based on electrostatic designs by three to four orders of magnitude [52]. This experiment verifies that the high SMA force contributes to achieving a high ON/OFF resistance ratio and that the restoring force generated by the SiO_2 reset layer is sufficient to overcome the surface force induced at the contact interface, releasing the cantilever from the forest to fully open the switch.

Based on the above result, the rest of the experiments were conducted with the dry-processed device in air. Figure 3c shows the dependence of the contact resistance

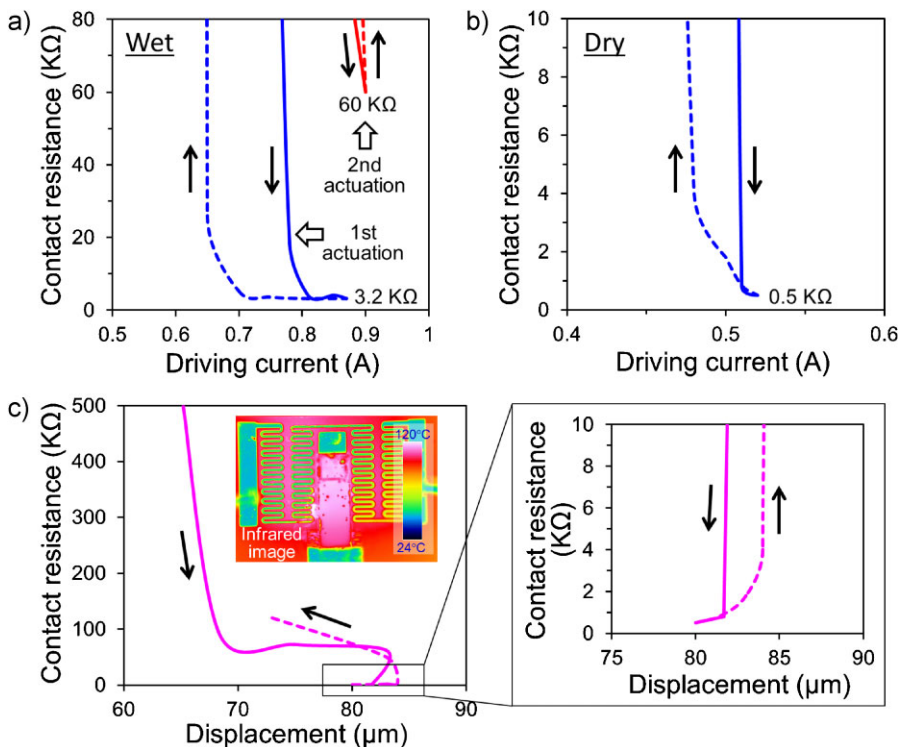


Figure 3 (online color at: www.pss-a.com) The dependence of contact resistance on the heater driving current for (a) wet-processed and (b) dry-processed devices. (c) The dependence of contact resistance on the SMA's displacement (from the point in the cold state with full upward bending) for the dry-processed device; the inset shows an infrared image of the device under operation.

on the vertical displacement of the cantilever tracked using the laser displacement sensor. For this measurement, the heater current was increased until observing a minimal ON-state resistance and then decreased while recording the displacement and the resistance. The laser spot of the sensor was directed to a location nearly at the edge of the free end of the cantilever. At a displacement of $65\ \mu\text{m}$, a readable resistance ($\sim 500\ \text{k}\Omega$) started to appear, at which point presumably initial contact between parts of the forest (that had thickness variation as noted earlier) and the copper was made. As the displacement was increased, the resistance continued to drop until reaching several tens of $\text{k}\Omega$, where the resistance was relatively stable for displacements of up to around $82\ \mu\text{m}$. The displacement beyond this level further decreased the contact resistance to $500\ \Omega$ as can be seen in the close-up plot in Fig. 3c. The small decrease of the displacement near the maximum point while the resistance still decreased may be related to the following condition: as the cantilever actuates downward, due to its curvature and angular motion, it may first touch the inner edge (the one closer to the SMA bonding region) of the CNT forest. This contact edge of the forest could act as a pivot axis for the cantilever to make a seesaw-like behavior, leading to an upward motion of the cantilever's tip that can decrease the displacement reading. The small increase of the displacement observed while decreasing the driving current can also be explained with the same hypothetical effect. Figure 4 shows variations of the signal current (I_{sig}) generated by applying a constant signal voltage ($V_{\text{sig}} = 0.2\ \text{V}$) between terminals 1 and 2 observed while displacing the cantilever with the driving current. This result clearly indicates that the ON-state I_{sig} depends on the displacement, *i.e.*, the contact force applied by the cantilever. This dependence can be understood considering the fact that CNTs are physically flexible, and thus increasing the force may result in more new contacts established with CNTs (while maintaining the existing contacts with other CNTs that are deformed by the force), lowering the contact resistance [53] and increasing

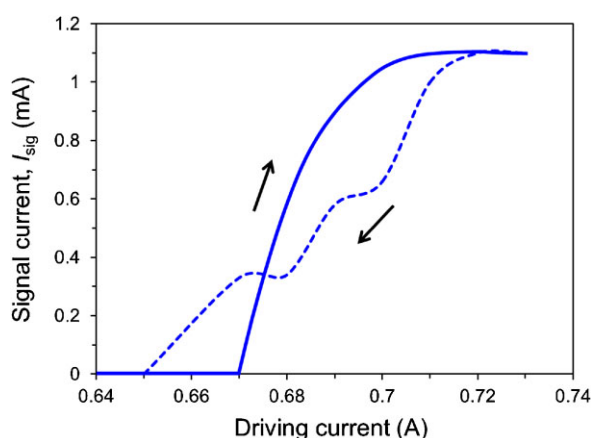


Figure 4 (online color at: www.pss-a.com) I_{sig} vs. heater driving current for the dry-processed device operated with a constant V_{sig} of $0.2\ \text{V}$, showing a dependence of I_{sig} on the actuation level of the SMA.

I_{sig} . The result in Fig. 4 also shows a transistor-like nonlinear response; I_{sig} rapidly increases at a threshold level of the input driving current (or that of the resultant displacement or force) that the contact is established, and its dependence diminishes when the displacement/force reaches a certain level (corresponding to a driving current of $\sim 0.7\ \text{A}$ in this test).

To assess the device ability and limitation in high-power operations, we conducted a destructive test, in which V_{sig} and I_{sig} fed to the ON-state switch were increased until the contact failed. Figure 5 shows the results of the tests for four different current levels (approximately 100, 200, 300, and $>400\ \text{mA}$) in which I_{sig} was increased and then decreased by adjusting V_{sig} . As shown, the cases with the maximum I_{sig} of up to $300\ \text{mA}$ (Fig. 5a, b, and c) showed consistent I - V behaviors. The result in Fig. 5d indicates that I_{sig} similarly increased to $400\ \text{mA}$ and more, corresponding to an input power of more than $5\ \text{W}$, but started to drop at $470\ \text{mA}$ while still increasing V_{sig} , and that the decreasing I - V path did not follow the increasing path unlike the other three cases. An optical observation verified that the copper layer on the bottom side of the cantilever had partly burnt and portions of the CNT forest were stuck to the cantilever side. This failure level of I_{sig} is significantly higher than those reported for gold contacts in MEMS (*e.g.*, $10\ \text{mA}$ [7]). The contact resistance was calculated from the above results (V_{sig} divided by the resultant I_{sig}) and plotted as a function of I_{sig} in Fig. 5e. This graph clearly shows that the contact resistance has a dependence on I_{sig} (or V_{sig}), more on the lower I_{sig} side, exhibiting a decreasing trend with which a power function fits well as displayed on the figure. This trend is advantageous in terms of the targeted application area. Figure 5e also shows that the resistance at the peak I_{sig} in Fig. 5c, the case tested with the highest peak I_{sig} ($300\ \text{mA}$) showing repeatable response, is $34.9\ \Omega$; this level is significantly lower than the minimum value ($286\ \Omega$) reported for the device that used a CNT-forest contact [37]. It also shows that the contact failed when it reached $30.6\ \Omega$ corresponding to the peak I_{sig} in Fig. 5d. The nonlinear dependence of the resistance shown in Fig. 5e and its reversibility imply a possibility for using the contact of a CNT forest and copper as a varistor-like component, in which its base resistance level is adjustable with the contact force generated by the actuator (Figs. 3c and 4). A similar dependence of the resistance on the signal current was reported for metallic contacts of a MEMS switch operated in air [54]. Although the mechanism of the dependence observed in our device is not clear, since its operating ambient was air as well, it might be associated with breakdown of an insulating film (formed on the copper surface) as suggested in the report; further study is necessary to analyze this characteristic of the contact.

The dynamic response of the switch was characterized using a feedback-looped set-up described in Section 2. A typical temporal behavior of the switch resistance is shown in Fig. 6, along with the driving-voltage waveform applied to the heater for the SMA actuation, showing an ON-OFF cycle

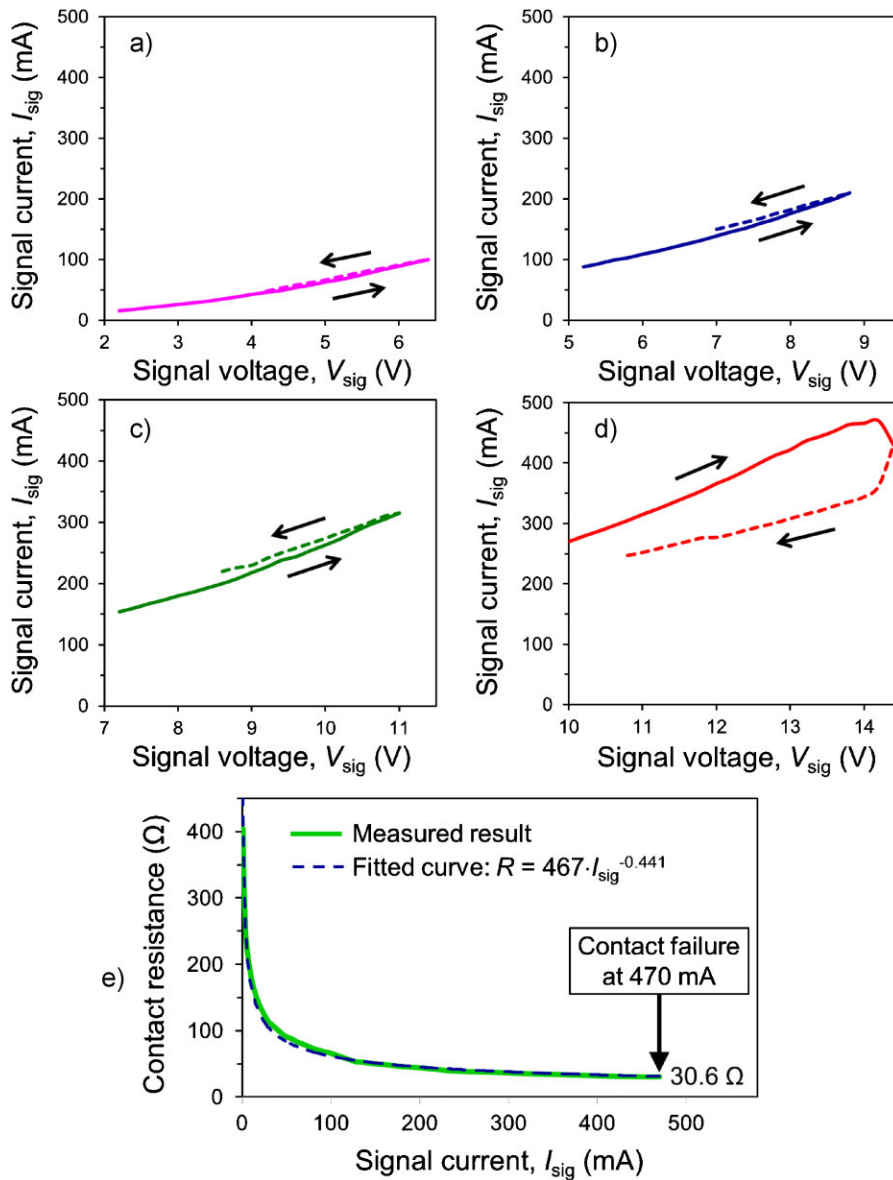


Figure 5 (online color at: www.pss-a.com) Signal I - V relationships with approximate maximum I_{sig} of (a) 100 mA, (b) 200 mA, (c) 300 mA, and (d) >400 mA; the last case shows a drop of the current indicating a failure of the contact. (e) Collective data of contact resistance calculated from the results in (a)–(d), showing a nonlinear dependence of the resistance on I_{sig} along with a fitted curve of a power function.

time of 2.3 s in this particular example. The shortest cycle time observed in this experiment was 1.7 s. These values are significantly smaller than the times observed in other SMA actuators with similar dimensions (*e.g.*, $\sim 8.2 \times$ faster than the case previously reported [43]) in the same environment (air without forced cooling). The cycle time is mainly defined by the speed of heat transfer to/from the SMA as well as the threshold temperature and response hysteresis of the material. Reducing the size of the SMA cantilever and selecting SMAs with lower threshold temperatures are expected to shorten the necessary heating time and improve the temporal response further. The integration of CNTs with SMA may be another possibility to improve the actuation frequency of SMA [55]. Nevertheless, the demonstrated speed may be sufficient for the targeted application area discussed earlier. Using the same control set-up, long-term

switching tests were performed. Figure 7a displays the trend of the ON-state resistance for over 1×10^6 cycles, showing relatively stable values at around 650–700 Ω for the entire test period. This experiment revealed that both the contact and the SMA actuator were still functional after the above cycles without showing noticeable degradations. Given the small strains (estimated to be $< 10^{-3}$) that the SMA is subject to during the actuation, the above result on the SMA seems to match the characteristics reported for macro-scale samples (millions of cycles for small strains) [56]. Figure 7b shows the top surface of the forest after the 10^6 cycles, at an area where one of the side edges of the cantilever was present. On the contact region in the image, the tips of the CNTs seem to have been more flattened and laterally oriented (along the direction of the arrow shown in the image) than the portion outside of the contact area that appears to maintain the

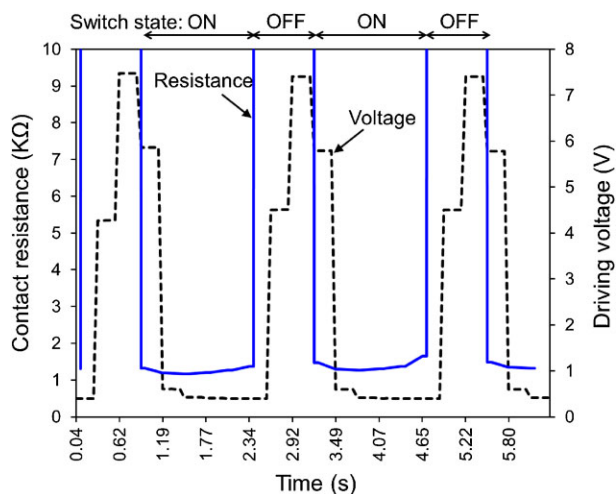


Figure 6 (online color at: www.pss-a.com) Temporal response in contact resistance of the device operated with feedback control and a voltage waveform used to drive the heater (small steps in the waveform were attributed to nonideal characteristics of the set-up used).

original surface morphology without directionality. This may be evidence that the physical flexibility of CNTs enabled vastly distributed contact points in the ON state of the switch, as opposed to the case with metallic MEMS switches that involves limited point contacts leading to premature failures as described earlier. A combination of this effect and other favorable features of CNT as well as those of SMA may have contributed to the performance demonstrated in this test and others discussed previously.

4 Conclusions We reported an SMA-based MEMS switch that utilized a contact combination of a CNT forest and copper. The device fabricated through dry processing showed much lower and consistent contact resistance compared to the case that used the wet process which resulted in densification of the forest structure. The dry-processed device exhibited contact resistances from $\sim 500 \Omega$ down to 35Ω or less for higher contact currents, providing high ON/OFF resistance ratios. This outcome was brought about by the use of the bulk-micromachined SMA actuator that enabled firm contacts with the CNT forest to achieve low ON-state resistances as well as releasing from the CNT forest while overcoming the surface force induced by the forest. The SMA actuator was feedback controlled to demonstrate an ON–OFF cycle time of 1.7 s, much faster than similarly sized SMA actuators reported in the past. The device was operated with input powers of $>5 \text{ W}$ and exhibited a failure at a current of 470 mA, both of which are higher than those involved in typical MEMS contact switches by one order of magnitude or more [7, 52]. A visual analysis revealed that the failure was associated with the copper layer on the SMA cantilever rather than the CNTs, suggesting that even higher powers could be fed to the contact safely with optimized copper thickness. Switching cycles of $>1 \times 10^6$ were

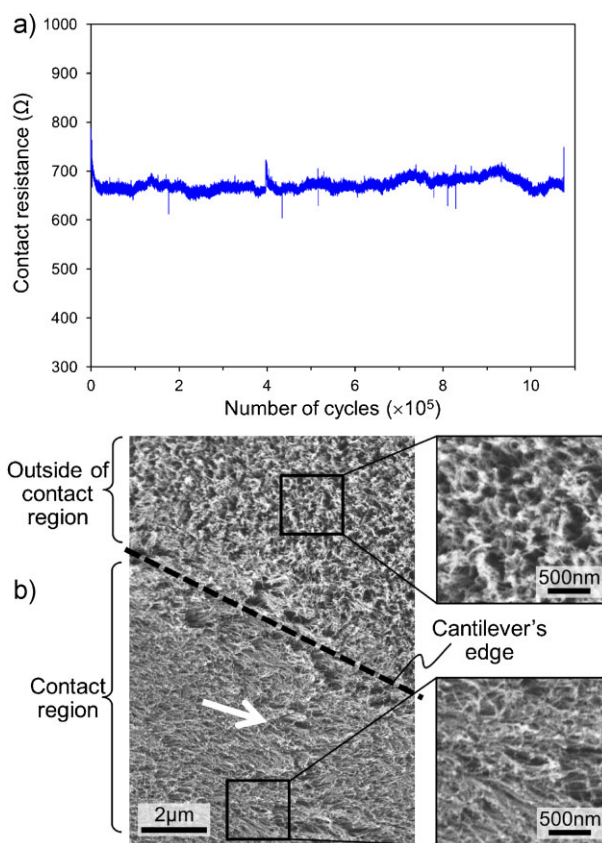


Figure 7 (online color at: www.pss-a.com) (a) Trend of the ON-state resistance for over 10^6 cycles. (b) SEM image and close-ups of two regions of the top surface of the CNT forest corresponding to the contact area (bottom) and outside of the area (top) after the 10^6 cycle test, showing different surface textures between them and laterally oriented nanotube tips for the former case.

demonstrated, without observing a sign of fatigue in the SMA actuation. This long-term experiment suggests that the CNT-copper contact tested may be a more reliable option than metal contacts widely used in MEMS. This is presumed to be enabled mainly by the excellent electrical, thermal, and mechanical properties of CNTs as well as the large effective contact area provided by the aligned CNT forest. The combination of this contact material and SMA actuator forms a robust contact switch potentially suitable for high-power applications. The CNT-copper contact was also observed to exhibit a varistor-like characteristic, implying another potential application of the contact material.

Acknowledgements We thank Dr. Edmond Cretu for providing access to the NI ELVIS board. This work was partially supported by Natural Sciences and Engineering Research Council of Canada, Canada Foundation for Innovation, British Columbia Knowledge Development Fund, and CMC Microsystems. K. Takahata is supported by the Canada Research Chairs program. M. S. Mohamed Ali acknowledges financial support from Ministry of Higher Education Malaysia and Universiti Teknologi Malaysia.

References

- [1] B. McCarthy, G. G. Adams, N. E. McGruer, and D. Potter, *J. Microelectromech. Syst.* **11**, 276–283 (2002).
- [2] S. Zhou, X.-Q. Sun, and W. N. Carr, *J. Micromech. Microeng.* **9**, 45–50 (1999).
- [3] G. M. Rebeiz and J. B. Muldavin, *IEEE Microw. Mag.* **2**, 59–71 (2001).
- [4] P. G. Steeneken and O. Wunnicke, in: 24th IEEE Int. Symp. on Power Semiconductor Devices and ICs, Bruges, Belgium (2012), pp. 417–420.
- [5] Y.-H. Song, C.-H. Han, M.-W. Kim, J. O. Lee, and J.-B. Yoon, *J. Microelectromech. Syst.* **21**, 1209–1217 (2012).
- [6] F. Ke, J. Miao, and J. Oberhammer, *J. Microelectromech. Syst.* **17**, 1447–1459 (2008).
- [7] S. T. Patton and J. S. Zabinski, *Tribol. Lett.* **18**, 215–230 (2005).
- [8] M.-A. Grétilat, F. Grétilat, and N. F. de Rooij, *J. Micromech. Microeng.* **9**, 324–331 (1999).
- [9] C. L. Goldsmith, Z. Yao, S. Eshelman, and D. Denniston, *IEEE Microw. Guided Wave Lett.* **8**, 269–271 (1998).
- [10] M. Park, B. A. Cola, T. Siegmund, J. Xu, M. R. Maschmann, T. S. Fisher, and H. Kim, *Nanotechnology* **17**, 2294–2303 (2006).
- [11] E. J. J. Kruglick and K. S. J. Pister, *J. Microelectromech. Syst.* **8**, 264–271 (1999).
- [12] R. A. Coutu, P. E. Kladitis, K. D. Leedy, and R. L. Crane, *J. Micromech. Microeng.* **14**, 1157–1164 (2004).
- [13] L. L. W. Chow, J. L. Volakis, K. Saitou, and K. Kurabayashi, *IEEE Electron Device Lett.* **28**, 479–481 (2007).
- [14] A. Cao, P. Yuen, and L. Lin, *J. Microelectromech. Syst.* **16**, 700–708 (2007).
- [15] Y.-H. Song, D.-H. Choi, H.-H. Yang, and J.-B. Yoon, *J. Microelectromech. Syst.* **20**, 204–212 (2011).
- [16] H.-S. Lee, C. H. Leung, J. Shi, S.-C. Chang, S. Lorincz, and I. Nedelescu, *J. Microelectromech. Syst.* **11**, 147–153 (2002).
- [17] J. Oberhammer and G. Stemme, *J. Microelectromech. Syst.* **15**, 1235–1242 (2006).
- [18] W. Simon, B. Schauwecker, A. Lauer, A. Wien, and I. Wolff, *Int. J. RF Microw. Comput.-Aid. Eng.* **14**, 329–337 (2004).
- [19] H. Kim, J. Kang, Y. Kim, B. H. Hong, J. Choi, and S. Iijima, *J. Nanosci. Nanotechnol.* **11**, 4 (2011).
- [20] N. Grobert, *Mater. Today* **10**, 28–35 (2007).
- [21] Z. Yao, C. Kane, and C. Dekker, *Phys. Rev. Lett.* **84**, 2941–2944 (2000).
- [22] B. Q. Wei, R. Vajtai, and P. M. Ajayan, *Appl. Phys. Lett.* **79**, 1172 (2001).
- [23] Y.-H. Li, J. Wei, X. Zhang, C. Xu, D. Wu, L. Lu, and B. Wei, *Chem. Phys. Lett.* **365**, 95–9100 (2002).
- [24] C. Hierold, *Carbon Nanotube Devices: Properties, Modeling, Integration and Applications* (Wiley-VCH, Weinheim, Germany, 2008).
- [25] L. Dong, S. Youkey, J. Bush, J. Jiao, V. M. Dubin, and R. V. Chebiam, *J. Appl. Phys.* **101**, 024320 (2007).
- [26] J. Robertson, G. Zhong, C. S. Esconjauregui, B. C. Bayer, C. Zhang, M. Fouquet, and S. Hofmann, *Jpn. J. Appl. Phys.* **51**, 01AH01 (2012).
- [27] N. R. Franklin, Y. Li, R. J. Chen, A. Javey, and H. Dai, *Appl. Phys. Lett.* **79**, 4571 (2001).
- [28] Y. Hayamizu, T. Yamada, K. Mizuno, R. C. Davis, D. N. Futaba, M. Yumura, and K. Hata, *Nature Nanotechnol.* **3**, 289–294 (2008).
- [29] D. N. Hutchison, N. B. Morrill, Q. Aten, B. W. Turner, B. D. Jensen, L. L. Howell, R. R. Vanfleet, and R. C. Davis, *J. Microelectromech. Syst.* **19**, 75–82 (2010).
- [30] Y. Hanein, *Phys. Status Solidi B* **247**, 2635–2640 (2010).
- [31] N. R. Franklin, Q. Wang, T. W. Tomblor, A. Javey, M. Shim, and H. Dai, *Appl. Phys. Lett.* **81**, 913 (2002).
- [32] C. Wang, K. Takei, T. Takahashi, and A. Javey, *Chem. Soc. Rev.*, DOI: 10.1039/c2cs35325c (2012).
- [33] B. R. Burg, T. Helbling, C. Hierold, and D. Poulikakos, *J. Appl. Phys.* **109**, 064310 (2011).
- [34] K. Chikkadi, C. Roman, L. Durrer, T. Süss, R. Pohle, and C. Hierold, *Procedia Engineering* **47**, 1374–1377 (2012).
- [35] J. Cao, C. Nyffeler, K. Lister, and A. M. Ionescu, *Carbon* **50**, 1720–1726 (2012).
- [36] A. Arun, H. Le Poche, T. Idda, D. Acquaviva, M. F.-B. Badia, P. Pantigny, P. Salet, and A. M. Ionescu, *Nanotechnology* **22**, 025203 (2011).
- [37] J. Choi, J.-I. Lee, Y. Eun, M.-O. Kim, and J. Kim, *Adv. Mater.* **23**, 2231–2236 (2011).
- [38] Y. Wang, Z. Li, D. T. McCormick, and N. C. Tien, *Sens. Actuators A* **103**, 231–236 (2003).
- [39] W. Shi, N. C. Tien, and Z. Li, *J. Microelectromech. Syst.* **16**, 1173–1184 (2007).
- [40] M. Glickman, P. Tseng, J. Harrison, T. Niblock, I. B. Goldberg, and J. W. Judy, *J. Microelectromech. Syst.* **20**, 842–851 (2011).
- [41] H.-C. Lee, J.-Y. Park, and J.-U. Bu, *IEEE Microw. Wireless Comp. Lett.* **15**, 202–204 (2005).
- [42] H. Kahn, M. A. Huff, and A. H. Heuer, *J. Micromech. Microeng.* **8**, 213–221 (1998).
- [43] M. S. Mohamed Ali and K. Takahata, *Sens. Actuators A* **163**, 363–372 (2010).
- [44] M. S. Mohamed Ali and K. Takahata, *J. Micromech. Microeng.* **21**, 075005 (2011).
- [45] B. Bhattacharya and O. P. Patel, *Sens. Transducers J.* **130**, 103–117 (2011).
- [46] J. Barth, B. Krevet, and M. Kohl, *Smart Mater. Struct.* **19**, 094004 (2010).
- [47] J.-E. Wong, J. H. Lang, and M. A. Schmidt, in: *Proc. IEEE, 13th Annu. Int. Conf. on Micro-Electro Mechanical Systems* (Cat. No.00CH36308) (IEEE, Miyazaki, Japan, 2000), pp. 633–638.
- [48] D. N. Futaba, K. Hata, T. Yamada, T. Hiraoka, Y. Hayamizu, Y. Kakudate, O. Tanaike, H. Hatori, M. Yumura, and S. Iijima, *Nature Mater.* **5**, 987–994 (2006).
- [49] W. Khalid, M. S. M. Ali, M. Dahmardeh, Y. Choi, P. Yaghoobi, A. Nojeh, and K. Takahata, *Diam. Relat. Mater.* **19**, 1405–1410 (2010).
- [50] M. Dahmardeh, A. Nojeh, and K. Takahata, *J. Appl. Phys.* **109**, 093308 (2011).
- [51] C. T. Wirth, S. Hofmann, and J. Robertson, *Diam. Relat. Mater.* **17**, 1518–1524 (2008).
- [52] S. K. Thakur, K. A. Sumithra Devi, and I. Ranjitha, in: *IEEE Applied Electromagnetics Conference (AEMC)*, Kolkata, India (2009), pp. 1–4.
- [53] F. Wakaya, K. Katayama, and K. Gamo, *Microelectron. Eng.* **67–68**, 853–857 (2003).
- [54] B. D. Jensen, L. L.-W. Chow, K. Huang, K. Saitou, J. L. Volakis, and K. Kurabayashi, *J. Microelectromech. Syst.* **14**, 935–946 (2005).
- [55] B. C. Bayer, S. Sanjabi, C. Baecht, C. T. Wirth, S. Esconjauregui, R. S. Weatherup, Z. H. Barber, S. Hofmann, and J. Robertson, *Thin Solid Films* **519**, 6126–6129 (2011).
- [56] D. C. Lagoudas, D. A. Miller, L. Rong, and P. K. Kumar, *Smart Mater. Struct.* **18**, 085021 (2009).